Polymer 208 (2020) 122925

Contents lists available at ScienceDirect

Polymer

journal homepage: http://www.elsevier.com/locate/polymer

Synthesis of aerogel foams through a pressurized sol-gel method

Sadeq Malakooti [a,2], Ethan Zhao [a,b,1,2], Nicholas Tsao [a,c,1,2], Ning Bian [a], Rushi U. Soni [d], ABM Shaheen ud Doulah [d], Chariklia Sotiriou-Leventis [d], Nicholas Leventis [e,*], Hongbing Lu [a,**]

[a] Department of Mechanical Engineering, The University of Texas at Dallas, Richardson, TX 75080, USA
[b] Allen High School, Allen, TX 75002, USA
[c] St. Mark's School of Texas, Dallas, TX 75230, USA
[d] Department of Chemistry, Missouri University of Science and Technology, Rolla, MO 65409, USA
[e] Aspen Aerogels, Inc., 30 Forbes Road, Bldg B, Northborough, MA 01532, USA

ARTICLE INFO

Keywords:
Aerogels
Foams
Porous materials
Pressurized sol-gel
Polyurethane

ABSTRACT

We report monolithic aerogel foams as solid materials with hierarchical porosity created by a foam-like structure embedded in the skeletal framework of a regular aerogel. The foam-like structure is prepared without chemical foaming agents or templates, resulting in a less expensive, more efficient, and more readily adaptable process. Specifically, pressurized air (7 bar) is injected into a suitable sol, which is allowed to gel under pressure, followed by slow depressurization. Voids are created from the air bubbles formed during depressurization. The model material used for validation of the technique is based on poly(isocyanurate-urethane) aerogels (PIR-PUR) and selected material properties of the resulted aerogel foams are compared with those of their pristine aerogel counterparts. With an eye on scalability, all wet-gels were dried under ambient conditions. Aerogel foams exhibit lower bulk densities by about 25%, and higher porosities by about 10% in comparison with their pristine PIR-PUR aerogel counterparts. Interestingly, the thermal conductivities of aerogel foams were found reduced significantly (by 25%) from 0.104 to 0.077 $Wm^{-1}K^{-1}$ compared to the corresponding pristine aerogels. In addition, aerogel foams absorb 36% w/w more oil and show better oil retention in comparison with regular PIR-PUR aerogel samples made from the same sols. As this technique does not alter the chemical composition of the aerogel, it is anticipated that it can be used for a variety of different types of aerogels and formulations in order to lower their bulk density and improve desired physical properties such as thermal conductivity.

1. Introduction

Aerogels are a class of porous materials characterized by their low bulk density, high open porosity and high specific surface area [1]. They are typically synthesized through a sol-gel process at atmospheric pressure followed by drying of the resulting wet-gels with a supercritical fluid (SCF), most commonly CO_2 [1,2]. On the other hand, solid foams are a different class of porous materials formed by pockets of gas trapped in a solid matrix, often again characterized by low bulk densities and high macroporosity [3]. Foaming is an important industrial process, which typically provides lighter and more cost-effective materials than in their nonfoam state [4]. The result of an aerogel foaming process, which we refer to as an "aerogel foam," merges the open porosity of an aerogel with the "closed" porosity of foams creating a novel multiscale, random, yet hierarchical open-pore structure, in which larger voids (pores) are interconnected in all directions (3D) by the innate aerogel pores. Existing manufacturing techniques utilize chemical foaming agents and methods involving aerogel synthesis within the macropores of prefabricated polymer templates, resulting in extremely specific procedures not suitable for the industrial scale [5–7]. These procedures can involve large amounts of sacrificial chemicals and therefore are expensive [6,8].

Our approach for the synthesis of aerogel foams without the use of chemical agents or templates involves gelation under high pressure through air injection into a specially designed mold. High pressure induces air dissolution into the sol, which generates bubbles and creates a

* Corresponding author.
** Corresponding author.
E-mail addresses: nleventis@aerogel.com (N. Leventis), hongbing.lu@utdallas.edu (H. Lu).
[1] High school summer researcher.
[2] These authors contributed equally to this work.

https://doi.org/10.1016/j.polymer.2020.122925
Received 12 June 2020; Received in revised form 3 August 2020; Accepted 10 August 2020
Available online 15 August 2020

foam-like structure during depressurization. Our procedure does not alter the chemical composition of the aerogel, so it could potentially be used for a variety of different aerogel types and formulations. Therefore, without loss of generality, the method is demonstrated here with a special type of a poly(isocyanurate-urethane) aerogel (PIR-PUR) [9,10]. The newly synthesized aerogel foams were characterized in terms of bulk density, porosity, thermal conductivity and oil absorption capabilities in comparison with their regular aerogel counterparts prepared from the same sol under atmospheric pressure.

2. Results and discussion

2.1. Pressurized sol-gel synthesis of PIR-PUR aerogel foams

The sol formulation (Fig. 1a) was adopted from Donthula et al. [10]. An aliphatic triisocyanate (Desmodur N3300A) and ethylene glycol (EG) were separately dissolved in anhydrous acetone and acetonitrile (the exact ratios are listed in Table S1 of the Supporting Information). A schematic of the pressure vessel and the synthetic protocol are shown in Fig. 1b and c, respectively. A photograph of the pressure mold is shown

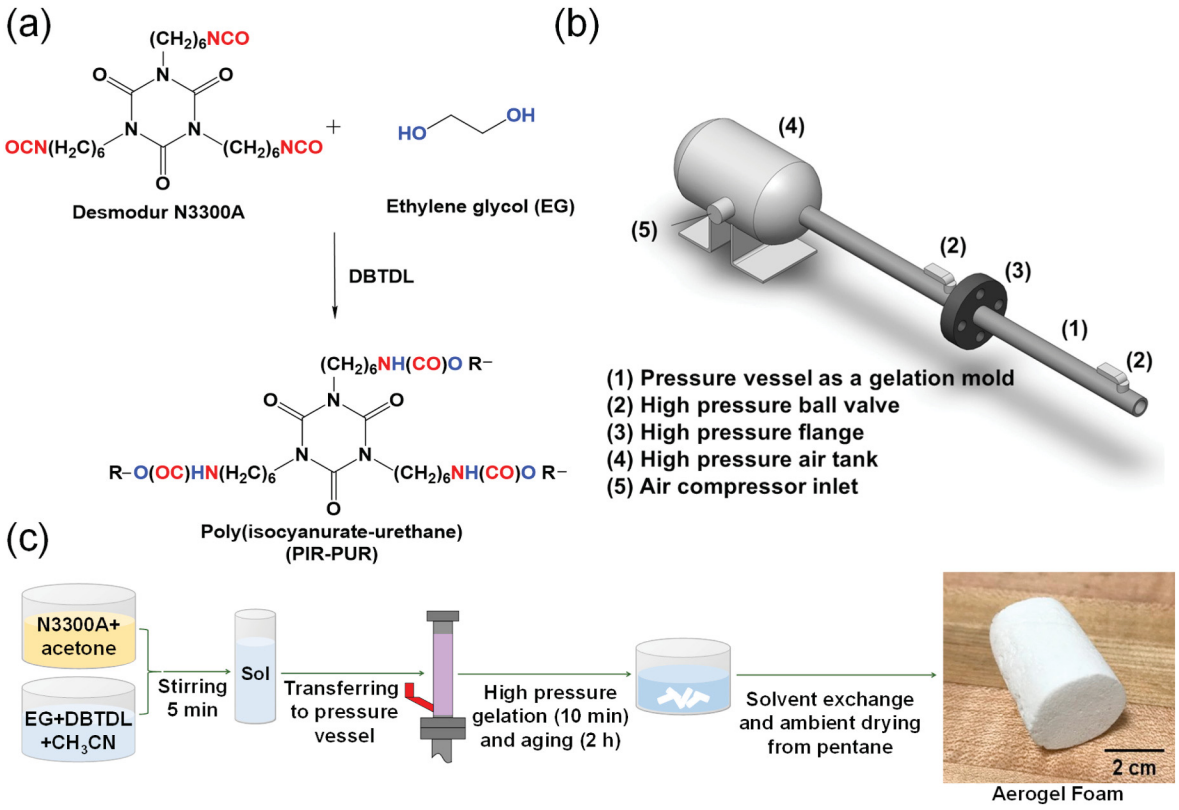

Fig. 1. (a) Reaction pathway to PIR-PUR aerogels; (b) Schematic of the pressure vessel used as a mold (for a photograph see Fig. S2 in Supporting Information); (c) Preparation procedure of the PIR-PUR aerogel foams.

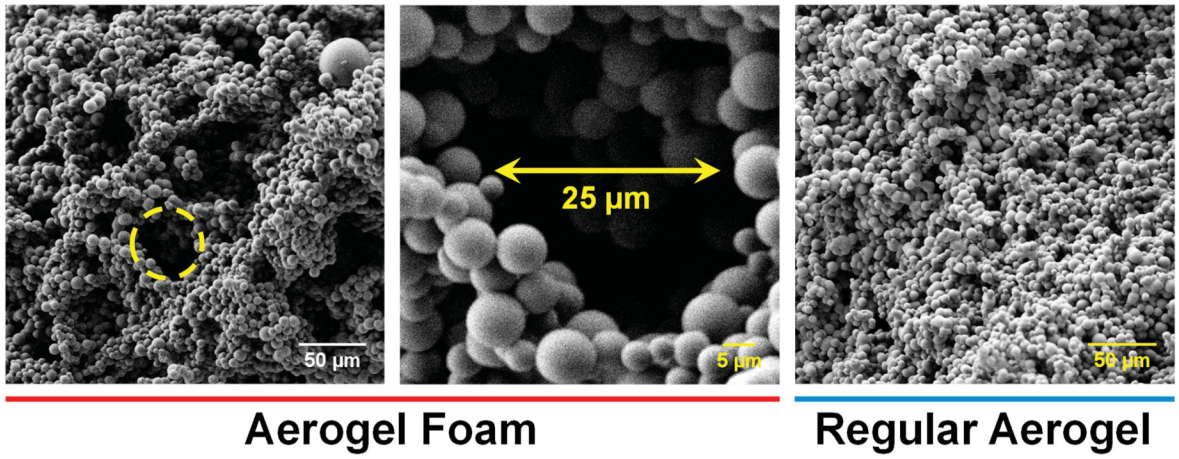

Fig. 2. SEM images of an aerogel foam (PIR-PUR-P1 sample) in comparison with a regular PIR-PUR aerogel.

Table 1
General material properties of regular PIR-PUR and aerogel foams[a].

Name	*Bulk Density* (ρ_b, g/cm^3)	*Skeletal Density* (ρ_s, g/cm^3)	*Linear Shrinkage*[b] (%)	*Porosity*[c] (%)
Regular Aerogel (PIR-PUR)	0.345 ± 0.009	1.215 ± 0.003	19	72
Aerogel Foam (PIR-PUR-P-1)	0.250 ± 0.007	1.244 ± 0.003	20	80
Aerogel Foam (PIR-PUR-P-2)	0.263 ± 0.014	1.240 ± 0.003	21	79
Aerogel Foam (PIR-PUR-P-3)	0.247 ± 0.002	1.236 ± 0.002	21	80

[a] Average of three measurements.
[b] Linear Shrinkage = 100 × [(Mold diameter – Sample diameter)/Mold diameter].
[c] Porosity = 100 × [(ρ_s−ρ_b)/ρ_s].

in Figure S2 of the Supporting Information. The two solutions were combined and stirred for 5 min at room temperature. Next, the correct amount of catalyst (dibutyltin dilaurate; DBTDL, see Table S1 in Supporting Information) was added, and the resulting sol was stirred for an additional 5 min. Subsequently, the sol was poured into the gelation vessel, which was then pressurized with air to 7 bar, and it was allowed to gel and age for 2 h at room temperature. A portion of the same sol (5 mL) was set aside in an unpressurized clear syringe for comparison. Both kinds of gels were post-processed in the same way. After aging, the high-pressure ball valve (see Fig. 1b) was loosened and tightened repeatedly to allow the vessel to gradually depressurize in stages. The sample was allowed to equilibrate for several minutes during each depressurization step. The total depressurization process lasted for approximately 45 min, and finally the gel was removed from the mold into an acetone-acetonitrile mixture. The gelation solvent was exchanged one more time with acetone, then with acetonitrile and finally with pentane for a period of 8 h in each bath. Those wet-gels were dried directly from pentane at room temperature under ambient pressure. The drying process was completed by placing the samples in a convection oven at 50 °C for 2 h.

2.2. General material and microstructural properties

The general material properties such as skeletal densities, bulk densities and porosities are listed in Table 1. The bulk densities were calculated from the sample dimensions and masses. The regular PIR-PUR aerogel sample (gelled under atmospheric pressure) had a bulk density of 0.345 g/cm^3. At the same monomer concentration, foamed samples had about 30% lower bulk densities, as low as 0.247 g/cm^3. As expected, the skeletal densities of the foamed samples were close to the skeletal density of the regular aerogel sample. Linear shrinkage was calculated by comparing the diameters of the samples with the inner diameter of the molds and it was found similar (at about 20%) between the regular and foamed samples. No significant syneresis was observed during gelation and aging. For all samples, the main shrinkage event took place during the ambient-pressure drying process. Porosities were calculated using the bulk and skeletal densities. Following the trend in bulk densities, the pressurized sol-gel approach increased the porosity by approximately 10%.

It is noted that the materials we describe fall between aerogels and xerogels: they have been prepared by ambient pressure drying, therefore they might not be considered as aerogels, but they have not been dried from the gelation solvent either, and therefore they may not be considered as xerogels. A more appropriate classification would have been as “ambigels,” [11]. However, based on Leventis’ previous work using supercritical drying, this particular formulation has a bulk density 0.32 g/cm3. As the bulk density and porosity of the materials of this study are close to the values of their supercritically-dried counterpart (only about 6% higher), we have opted to refer to them as “aerogels” and “aerogel foams.” It should also be noted that our aerogel foams have even lower bulk densities than their supercritical dried counterpart.

The morphology of the foamed samples was studied using scanning electron microscopy (SEM, Fig. 2 and Fig. S1 in the Supporting Information). It is immediately apparent that the skeletal particle size of the regular aerogel and the aerogel foam were approximately equal, and therefore it was concluded that the mechanism of particle formation (phase separation of liquid oligomers, followed by spherodization and solidification [12,13]) was not affected by the sol pressurization.

Quantitatively, several random particles were selected from the SEM images and the particle diameters were used in order to construct the particle size distribution curves of Fig. 3. The particle size distribution in the aerogel foam was slightly broadened compared to that of the regular aerogel samples. However, the average particle diameter of both types of aerogels was close to 8 μm.

The air dissolved in the sol during gelation formed bubbles during depressurization, leading to the formation of macrovoids surrounded by the pore structure of the regular aerogel. Based on Fig. 2, the size of a typical macrovoid was around 25 μm. It is worth mentioning that the processes of bubble nucleation (void formation) and growth (phase separation) may both be affected by many factors including gas

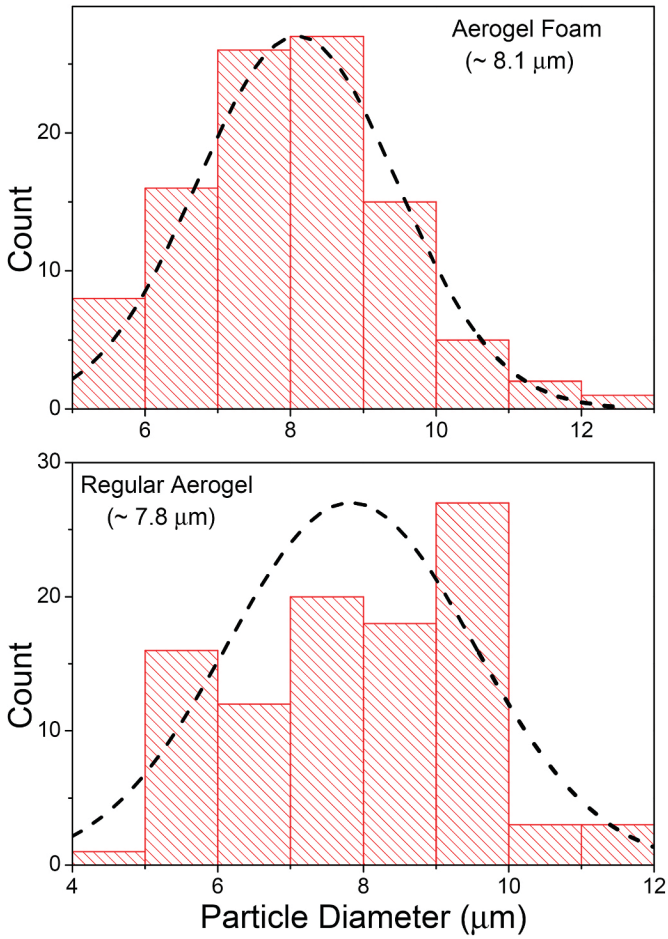

Fig. 3. Particle size distribution of a regular PIR-PUR and of an aerogel foam.

solubility, diffusivity, and bubble surface tension, which are also functions of the foaming temperature and pressure. However, the size of the voids depends on the pressure difference between the inside of the bubble and the surrounding medium. Therefore, either by increasing the sol internal pressure or lowering the external pressure during the depressurization stage, the size of the macrovoids can be potentially controlled. Larger macrovoids either due to supercritical drying or by increasing the pressure difference between the interior of the bubble and the surrounding medium can lead to aerogel materials with higher porosities.

SEM analysis of a material's morphology is a qualitative characterization method and in most cases the results are simply articulated verbally. A thorough quantitative analysis would require numerical image processing which is outside the scope of this report. In order to quantify the effect of the pressurized gelation on the pore morphology of aerogel foams versus that of a regular aerogel, the SEM images in Fig. 2 were analyzed using the ImageJ software package (Radial Profile Plot) [14] as follows (see Fig. 4): First, the integrated intensity at a given distance from a randomly selected reference point was defined by the sum of the pixel values around a circle with the reference point as its center and the given distance as its radius (see Fig. 4, Inset); Subsequently, the integrated intensities were divided by the number of pixels in the circle to obtain the normalized integrated intensities. Of course, for this analysis to be valid, the SEM images had to be captured at the same magnification, same brightness, same exposure time, etc. The normalized integrated intensities were used as indicators of the radial particle distribution as a function of the radial distance from the center point of the SEM images. According to Fig. 4, there is a distinct peak in the radial profile of the regular PIR-PUR aerogels at 10–20 μm. With 8 μm average particle diameter (see above), this peak shows that aerogel particles, and therefore the porous space created in between, are distributed evenly at the vicinity of the center point of the SEM image. Since the selection of the center point was random, this assertion is valid for the entire material. This conclusion is consistent with the SEM image of the regular aerogels (Fig. 2). However, this picture is no longer valid in the aerogel foams: as data of Fig. 4 show, in that case we have three macrovoids around the SEM center point. Interestingly, the radial profiles of both the regular aerogel and the aerogel foam are converging as the sampling radius increases above 60 μm. However, the converging intensity value of aerogel foams is 34% lower than the corresponding value of a regular aerogel. That percent difference between the converged intensities is in the same range as the percent difference of bulk densities between regular PIR-PUR aerogel and aerogel foams. This observation suggests that the normalized integrated intensities can be used to quantify morphology related differences in nanostructured materials and we intend to explore it further.

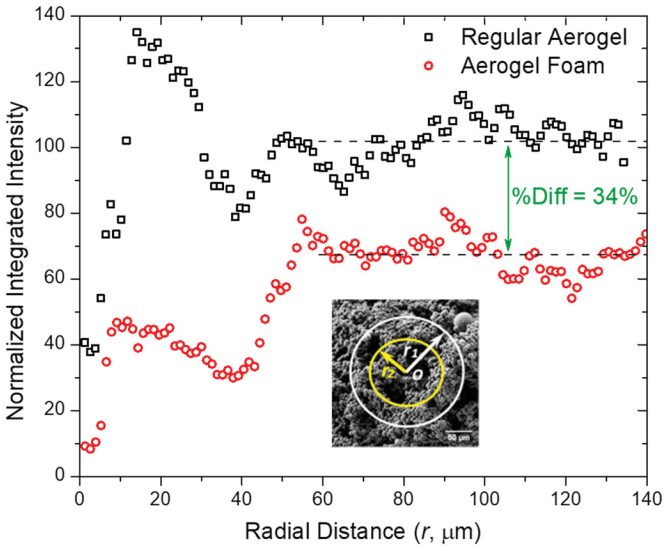

Fig. 4. Normalized integrated intensities of the regular aerogel and aerogel foam (PIR-PUR-P1) as a function of the radial distance, *r*, from a randomly selected center point (*O*) in the SEM – see Inset. (Data are used to quantify the void space distribution.)

2.3. Thermal properties

The thermal diffusivities, *R*, of a regular aerogel and aerogel foams were measured using the laser flash method as a non-contact, non-destructive, and highly accurate method [14,15]. The *R* values are listed in Table 2. Due to the increase in porosity and the presence of new voids in the aerogel foams relative to the regular aerogel, the air thermal diffusivity is expected to be higher in aerogel foams relative to regular aerogels. However, that increase in thermal diffusivities is apparently moderated by a reduction of the amount of solid material in the skeletal framework, and as a result the thermal diffusivities of the two materials remain within error about equal to one another (Fig. 5a). Thermal conductivities (k) were then calculated from the corresponding thermal diffusivities (R) using the relationship $k = R \times c_p \times \rho_b$, where c_p and ρ_b are the specific heat capacity and the bulk density, respectively. Here, the specific heat capacity was considered equal for all materials (1.711 ± 0.074 J g^{-1} K^{-1}) [12]. The thermal conductivities of the regular aerogel and aerogel foams are included in Table 2. Signifying the solid network contribution, the thermal conductivities of the aerogel foams were notably lower (by 25%) compared to the corresponding values of regular aerogels prepared with the same monomer concentration (Fig. 5b). This further underlines the fact that heat transfer between pore-filling air and the PIR-PUR walls of the aerogel foam is negligible [17]. Therefore, with a significant reduction in bulk density (about 30%), the heat transfer contribution of the PIR-PUR phase is significantly reduced and subsequently the total thermal conductivity in the aerogel foams is also reduced proportionally compared to the regular aerogel.

2.4. Oil absorption properties

Fig. 6 shows the percent mass gain of the regular aerogel and aerogel foam (PIR-PUR-P1) as a function of time when corresponding samples were submerged in engine oil (density of 0.8 g/cm^3). The aerogel foam shows a peak mass gain of 219%, which was reached in a little over 1 min. The peak mass gain for regular aerogel was 165%, which was reached at roughly the same time. Both samples maintained this peak mass gain. However, as it was expected, due to the higher porosity of aerogel foams, those samples were 36% more absorbent (29%

Table 2
Thermal diffusivity and thermal conductivity of a regular PIR-PUR aerogel and aerogel foams at room temperature.

Name	Thermal diffusivity, (mm^2 s^{-1})	Thermal conductivity, (W m^{-1} K^{-1})
Regular Aerogel (PIR-PUR)	0.177 ± 0.006	0.104 ± 0.006
Aerogel Foam (PIR-PUR-P1)	0.192 ± 0.001	0.082 ± 0.010
Aerogel Foam (PIR-PUR-P2)	0.169 ± 0.011	0.076 ± 0.007
Aerogel Foam (PIR-PUR-P3)	0.175 ± 0.008	0.074 ± 0.005

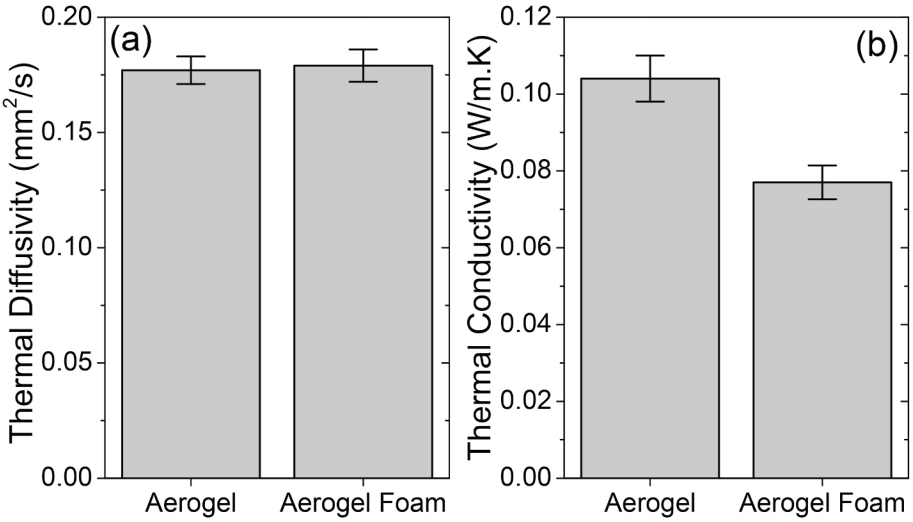

Fig. 5. (a) Average thermal diffusivity and (b) average thermal conductivity of the regular PIR-PUR aerogel and of the corresponding aerogel foams at room temperature.

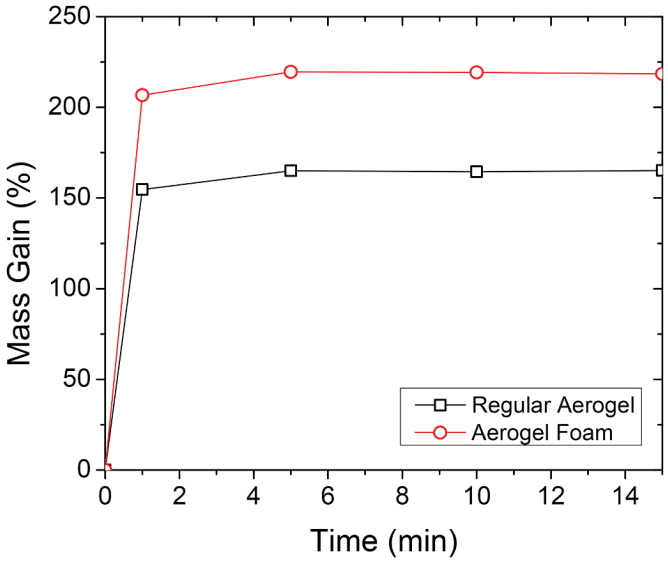

Fig. 6. Percent mass gain of the regular aerogel and aerogel foam (PIR-PUR-P1) upon submerging in engine oil as a function of time.

improvement in terms of volume uptake) than the regular aerogel samples. In fact, that increase in oil absorption capacity far exceeds the increase in porosity (10%), which might be attributed to greater swelling due to lower density. It is interesting to note that aerogel foams released a minimal amount of oil during the experiments, whereas the regular aerogel sample released a significantly larger volume of oil. Thus, aerogel foams demonstrate better oil retention and absorption than regular aerogels.

3. Conclusions

In summary, polymeric aerogels with foam-like porosity surrounded by regular structural characteristics of the corresponding aerogels were prepared using a pressurized sol-gel approach. The procedure of injecting high-pressure air into the gelation vessel containing a proper sol is indeed an environmentally friendly and low-cost method for producing aerogel foams. Aerogel foams exhibited significantly lower bulk density, higher porosity, and lower thermal conductivity compared to their regular aerogel counterparts. Further research will be conducted to control the effects of gelation temperature and injected air pressure. With aerogels demonstrating applications such as oil-spill cleaning, CO_2 capturing, blood fractionating, air freshener release, mosquito repellant release, filter for hemodialysis, and so on, it is speculated that aerogel foams will demonstrate further quantitative improvements in all these applications.

4. Experimental

Materials: Acetone, acetonitrile, and ethylene glycol were obtained from Fisher Scientific (Hampton, NH). Desmodur N330A was supplied by Covestro (Pittsburgh, PA). Dibutyltin dilaurate, 95% (DBTDL) was obtained from Alfa Aesar (Haverhill, MA). Five-millimeter plastic vials were used as molds. All purchased materials were used without further processing.

***Setup for gelation under pressure*:** A 6" threaded steel pipe was attached to a high-pressure vessel via a ball valve and a flange. The other end was closed with a steel cap. An air compressor was attached to the vessel through a pressure gauge. To reach higher pressures, a more powerful air compressor was attached to the gauge. Fig. S2 in the Supporting Information shows the setup for the pressurized so-gel synthesis. The sol is poured into the steel pipe when the ball valve is closed and then sealed with the steel cap. The total volume of the gelation vessel is roughly 100 mL. A total of 90 mL sol was used to allow space for the expansion of the pressurized sample.

Synthesis: Monomeric compounds Desmodur N3300A and ethylene glycol were dissolved separately in acetone and acetonitrile (exact amounts are listed in Table S1 of the Supporting Information). The two solutions were combined and stirred for 5 min at room temperature. Dibutyltin dilaurate catalyst was then added, and the solution was stirred for an additional 5 min. The solution was poured into the gelation vessel, where it was pressurized with an air compressor and allowed to gel and age for 2 h at room temperature. For sample removal, the cap of the gelation vessel was loosened and tightened repeatedly to allow gradual depressurization in stages. The sample was allowed to equilibrate for several minutes during each depressurization step, totaling approximately 45 min. The samples were then washed successively twice with acetone, acetonitrile, and finally pentane for a period of 8 h in each bath. Pentane-filled wet-gels were allowed to dry at room temperature and pressure for 24 h. The resulting aerogels were cured in a convection oven at 50 °C for 2 h. A 5 mL aliquot of each sol was set aside

in an unpressurized clear syringe and was left for gelation. These control samples were processed in the same way as the aerogel foams.

Basic material characterization: Bulk densities (ρ_b) were determined from the weight and the physical dimensions of the samples. Skeletal densities (ρ_s) were determined with helium pycnometry using a Micromeritics AccuPyc II 1340 instrument. Samples for skeletal density measurements were outgassed for 24 h at room temperature under vacuum before analysis. Porosities (Π) as a percent of empty space were determined from the ρ_b and ρ_s values via $\Pi = 100 \times [(\rho_s - \rho_b)/\rho_s]$.

***Scanning electron microscopy*:** SEM images were captured from Au/Pd (60/40) coated samples on a Hitachi Model S-4700 field emission microscope.

***Thermal conductivity*:** The total thermal conductivities of all samples were calculated at 23 °C via $k = R \times c_p \times \rho_b$, as has been described recently [16]. The thermal diffusivity, R, of each sample was determined at room temperature and atmospheric pressure with a Netzsch NanoFlash Model LFA 447 flash diffusivity instrument using disk samples (~1 cm in diameter, 2–3 mm thick) [9,18].

***Oil absorption capability*:** Two small beakers filled with engine oil (Castrol Ltd., Liverpool, UK) were prepared. The samples were lowered into the beakers, then allowed to soak for an allotted time period. The samples were then removed from the beaker and placed in Petri dishes, where they sat to dry for 1 min. After this drying interval, the samples were squeezed, and then were placed back into the oil.

CRediT authorship contribution statement

Sadeq Malakooti: Conceptualization, Methodology, Investigation, Validation, Visualization, Writing - original draft. **Ethan Zhao:** Investigation, Writing - original draft. **Nicholas Tsao:** Investigation, Writing - original draft. **Ning Bian:** Investigation, Writing - review & editing. **Rushi U. Soni:** Investigation, Writing - review & editing. **ABM Shaheen ud Doulah:** Investigation, Writing - review & editing. **Chariklia Sotiriou-Leventis:** Supervision, Resources, Writing - review & editing. **Nicholas Leventis:** Supervision, Resources, Writing - review & editing. **Hongbing Lu:** Conceptualization, Methodology, Supervision, Project administration, Funding acquisition, Resources, Writing - review & editing.

Declaration of competing interest

The authors declare the following financial interests/personal relationships which may be considered as potential competing interests: S. M. and H.L. are co-inventors on a provisional patent application (U.S. Patent Application No. 63/058,568) submitted by University of Texas at Dallas that concerns the aerogel foams and their preparation methods.

Acknowledgment

We thank the NSF under award numbers CMMI-1661246, CMMI-1636306, CMMI-1726435 and 1530603 (sub-contract to MS&T from Tufts University), and the Army Research Office (W911NF-14-1-0369) for financial support. H. Lu is also grateful for support by the Louis Beecherl Jr. Endowed Chair.

Appendix A. Supplementary data

Supplementary data to this article can be found online at https://doi.org/10.1016/j.polymer.2020.122925.

References

[1] A.C. Pierre, History of aerogels. Aerogels Handb., Springer, New York, NY, 2011, pp. 3–18, https://doi.org/10.1007/978-1-4419-7589-8_1.
[2] A.C. Pierre, A. Rigacci, SiO2 aerogels. Aerogels Handb., Springer New York, New York, NY, 2011, pp. 21–45, https://doi.org/10.1007/978-1-4419-7589-8_2.
[3] A.M. Kraynik, M.K. Neilsen, Elastic behavior of cellular solids. Encycl. Mater. Sci. Technol., Elsevier, 2001, pp. 2387–2389, https://doi.org/10.1016/b0-08-043152-6/00421-6.
[4] G. Wypych, Introduction. Handb. Foam. Blowing Agents, Elsevier, 2017, pp. 1–2, https://doi.org/10.1016/b978-1-895198-99-7.50003-9.
[5] N. Teo, S.C. Jana, Open cell aerogel foams via emulsion templating, Langmuir 33 (2017) 12729–12738, https://doi.org/10.1021/acs.langmuir.7b03139.
[6] N. Leventis, S. Mulik, X. Wang, A. Dass, V.U. Patil, C. Sotiriou-Leventis, H. Lu, G. Churu, A. Capecelatro, Polymer nano-encapsulation of templated mesoporous silica monoliths with improved mechanical properties, J. Non-Cryst. Solids 354 (2008) 632–644, https://doi.org/10.1016/j.jnoncrysol.2007.06.094.
[7] N. Teo, Z. Gu, S.C. Jana, Polyimide-based aerogel foams, via emulsion-templating, Polymer 157 (2018) 95–102, https://doi.org/10.1016/j.polymer.2018.10.030.
[8] S. Gu, S.C. Jana, Open cell aerogel foams with hierarchical pore structures, Polymer 125 (2017) 1–9, https://doi.org/10.1016/j.polymer.2017.07.085.
[9] C. Chidambareswarapattar, P.M. McCarver, H. Luo, H. Lu, C. Sotiriou-Leventis, N. Leventis, Fractal multiscale nanoporous polyurethanes: flexible to extremely rigid aerogels from multifunctional small molecules, Chem. Mater. 25 (2013) 3205–3224, https://doi.org/10.1021/cm401623h.
[10] S. Donthula, C. Mandal, T. Leventis, J. Schisler, A.M. Saeed, C. Sotiriou-Leventis, N. Leventis, Shape memory superelastic poly(isocyanurate-urethane) aerogels (PIR-PUR) for deployable panels and biomimetic applications, Chem. Mater. 29 (2017) 4461–4477, https://doi.org/10.1021/acs.chemmater.7b01020.
[11] J.P. Vareda, A. Lamy-Mendes, L. Durães, A reconsideration on the definition of the term aerogel based on current drying trends, Microporous Mesoporous Mater. 258 (2018) 211–216, https://doi.org/10.1016/j.micromeso.2017.09.016.
[12] S. Donthula, C. Mandal, J. Schisler, T. Leventis, M.A.B. Meador, C. Sotiriou-Leventis, N. Leventis, Nanostructure-dependent marcus-type correlation of the shape recovery rate and the young's modulus in shape memory polymer aerogels, ACS Appl. Mater. Interfaces 10 (2018) 23321–23334, https://doi.org/10.1021/acsami.8b06234.
[13] T. Taghvaee, S. Donthula, P.M. Rewatkar, H. Majedi Far, C. Sotiriou-Leventis, N. Leventis, K -Index, A descriptor, predictor, and correlator of complex nanomorphology to other material properties, ACS Nano 13 (2019) 3677–3690, https://doi.org/10.1021/acsnano.9b00396.
[14] (n.d. ImageJ. https://imagej.nih.gov/ij/. (Accessed 20 April 2020) accessed.
[15] S. Min, J. Blumm, A. Lindemann, A new laser flash system for measurement of the thermophysical properties, Thermochim. Acta 455 (2007) 46–49, https://doi.org/10.1016/j.tca.2006.11.026.
[16] S. Malakooti, G. Qin, C. Mandal, R. Soni, T. Taghvaee, Y. Ren, H. Chen, N. Tsao, J. Shiao, S.S. Kulkarni, C. Sotiriou-Leventis, N. Leventis, H. Lu, Low-cost, ambient-dried, superhydrophobic, high strength, thermally insulating, and thermally resilient polybenzoxazine aerogels, ACS Appl. Polym. Mater. 1 (2019) 2322–2333, https://doi.org/10.1021/acsapm.9b00408.
[17] K. Sakai, Y. Kobayashi, T. Saito, A. Isogai, Partitioned airs at microscale and nanoscale: thermal diffusivity in ultrahigh porosity solids of nanocellulose, Sci. Rep. 6 (2016) 1–7, https://doi.org/10.1038/srep20434.
[18] D.P. Mohite, S. Mahadik-Khanolkar, H. Luo, H. Lu, C. Sotiriou-Leventis, N. Leventis, Polydicyclopentadiene aerogels grafted with PMMA: II. Nanoscopic characterization and origin of macroscopic deformation, Soft Matter 9 (2013) 1531–1539, https://doi.org/10.1039/C2SM27606B.